Theory and Applications of Mathematics & Computer Science

(ISSN 2067-2764, EISSN 2247-6202)
http://www.uav.ro/applications/se/journal/index.php/tamcs

Theory and Applications of Mathematics & Computer Science 9 (1) (2019) 1 – 7

On Some Nonuniform Dichotomic Behaviors of Discrete Skew-product Semiflows

Claudia Luminiţa Mihiţ[a,b,*]

[a]*Department of Mathematics, Faculty of Mathematics and Computer Science, West University of Timişoara, V. Pârvan Blv. No. 4, 300223 Timişoara, Romania*
[b]*Department of Mathematics and Computer Science, Faculty of Exact Sciences, "Aurel Vlaicu" University of Arad, Elena Drăgoi Street no.2, 310330 Arad, Romania.*

Abstract

In this paper we approach concepts of nonuniform dichotomy for the case of discrete skew-product semiflows. Different characterizations of this properties are given from the point of view of invariant and strongly invariant projector families.

Keywords: discrete skew-product semiflow, nonuniform dichotomy, nonuniform exponential dichotomy.
2010 MSC: 34D05, 34D09.

1. Introduction

The (exponential) dichotomy is one of the most representative asymptotic properties studied for discrete dynamical systems in (Alonso *et al.*, 1999), (Babuţia & Megan, 2016), (Crai, 2016), (Elaydi & Janglajew, 1998), (Popa *et al.*, 2012), (Sasu & Sasu, 2013) from various perspectives.

In (Sasu, 2009) is approached the uniform exponential dichotomy for discrete skew-product flows and in (Biriş *et al.*, 2019) the authors investigate a generalization of the uniform exponential dichotomy property (the uniform exponential splitting) for discrete skew-product semiflows. Other significant results for the dichotomic behaviors of skew-product semiflows are obtained in (Biriş & Megan, 2016), (Chow & Leiva, 1996) and (Huy & Phi, 2010).

Regarding the nonuniform dichotomies, M. Megan, B. Sasu and A. L. Sasu ((Megan *et al.*, 2002)) prove interesting results for the nonuniform exponential dichotomy of evolution operators, using admissibility techniques. Also, different concepts of nonuniform exponential dichotomy and nonuniform polynomial dichotomy are studied in (Megan & Stoica, 2010) and (Stoica, 2016).

In this article, the properties of nonuniform dichotomy and nonuniform exponential dichotomy are treated for discrete variational systems, described through discrete skew-product semiflows. We prove criteria for the nonuniform exponential dichotomy, based on some results from (Przyluski & Rolewicz, 1984) and in particular we illustrate the characterizations for the nonuniform dichotomy.

*Corresponding author
Email address: mihit.claudia@yahoo.com; claudia.mihit@uav.ro (Claudia Luminiţa Mihiţ)

2. Preliminaries

In the following, we denote by Θ a metric space, by X a Banach space and by $\mathcal{B}(X)$ the Banach algebra of all bounded linear operators on X. The norms on X and on $\mathcal{B}(X)$ will be denoted by $\|\cdot\|$. Let I be the identity operator on X and $\Gamma = \Theta \times X$.

Definition 2.1. A mapping $S : \mathbb{N} \times \Theta \to \Theta$ is called *discrete semiflow* on Θ, if:

(ds_1) $S(0, \theta) = \theta$, for all $\theta \in \Theta$;

(ds_2) $S(m, S(n, \theta)) = S(m + n, \theta)$, for all $(m, n, \theta) \in \mathbb{N}^2 \times \Theta$.

Example 1. We consider $\Theta = \mathbb{N}$ and $S : \mathbb{N} \times \Theta \to \Theta$, $S(n, \theta) = n + \theta$. It is immediate to see that S is a discrete semiflow on Θ.

Definition 2.2. We say that $C : \mathbb{N} \times \Theta \to \mathcal{B}(X)$ is *discrete cocycle* over the discrete semiflow $S : \mathbb{N} \times \Theta \to \Theta$ if:

(dc_1) $C(0, \theta) = I$, for all $\theta \in \Theta$;

(dc_2) $C(m, S(n, \theta))C(n, \theta) = C(m + n, \theta)$, for all $(m, n, \theta) \in \mathbb{N}^2 \times \Theta$.

Example 2. Let $U : \{(m, n) \in \mathbb{N}^2 : m \geq n\} \to \mathcal{B}(X)$ be a discrete evolution operator on the Banach space X and $\Theta = \mathbb{N}$. Then $C_U : \mathbb{N} \times \Theta \to \mathcal{B}(X)$, given by

$$C_U(n, \theta) = U(n + \theta, \theta), \quad \text{for all} \quad (n, \theta) \in \mathbb{N} \times \Theta$$

is a discrete cocycle over the discrete semiflow considered in Example 1.

Definition 2.3. The mapping $\pi : \mathbb{N} \times \Gamma \to \Gamma$, given by

$$\pi(n, \theta, x) = (S(n, \theta), C(n, \theta)x),$$

where C is a discrete cocycle over a discrete semiflow S, is called *discrete skew-product semiflow on* Γ.

Definition 2.4. A mapping $P : \Theta \to \mathcal{B}(X)$ is said to be *family of projectors* if:

$$P^2(\theta) = P(\theta), \text{ for all } \theta \in \Theta.$$

If $P : \Theta \to \mathcal{B}(X)$ is a family of projectors, then $Q : \Theta \to \mathcal{B}(X)$, defined by $Q(\theta) = I - P(\theta)$ represents the *complementary family of projectors of* P.

Definition 2.5. A family of projectors $P : \Theta \to \mathcal{B}(X)$ is called

- *invariant* for a discrete skew-product semiflow $\pi = (S, C)$ if:

$$P(S(n, \theta))C(n, \theta) = C(n, \theta)P(\theta), \quad \text{for all } (n, \theta) \in \mathbb{N} \times \Theta;$$

- *strongly invariant* for a discrete skew-product semiflow $\pi = (S, C)$ if it is invariant for π and for all $(n, \theta) \in \mathbb{N} \times \Theta$, the restriction $C(n, \theta)$ is an isomorphism from $Ker\ P(\theta)$ to $Ker\ P(S(n, \theta))$.

Remark 1. If $P : \Theta \to \mathcal{B}(X)$ is a strongly invariant family of projectors for $\pi = (S, C)$, then there exists the mapping $D : \mathbb{N} \times \Theta \to \mathcal{B}(X)$ such that for all $(n, \theta) \in \mathbb{N} \times \Theta$ the bounded linear operator $D(n, \theta)$ is an isomorphism from $Ker\ P(S(n, \theta))$ to $Ker\ P(\theta)$ and

(i) $C(n, \theta)D(n, \theta)Q(S(n, \theta)) = Q(S(n, \theta))$;

(ii) $D(n, \theta)C(n, \theta)Q(\theta) = Q(\theta)$;

(iii) $Q(\theta)D(n, \theta)Q(S(n, \theta)) = D(n, \theta)Q(S(n, \theta))$,

for all $(n, \theta) \in \mathbb{N} \times \Theta$.

3. Nonuniform dichotomic behaviors of discrete skew-product semiflows

Let $\pi = (S, C)$ be a discrete skew-product semiflow and $P : \Theta \to \mathcal{B}(X)$ an invariant family of projectors for π.

Definition 3.1. The pair (π, P) is called *nonuniformly dichotomic* if there exists a mapping $N : \Theta \to \mathbb{R}_+^*$ such that:

(nd_1) $\|C(n,\theta)P(\theta)x\| \leq N(\theta)\|P(\theta)x\|$;
(nd_2) $\|Q(\theta)x\| \leq N(\theta)\|C(n,\theta)Q(\theta)x\|$,

for all $(n, \theta, x) \in \mathbb{N} \times \Gamma$.

In particular, if N is a constant function, then (π, P) is named *uniformly dichotomic*.

Remark 2. The pair (π, P) admits a nonuniform dichotomy if and only if there exists $N : \Theta \to \mathbb{R}_+^*$ with:

(nd_1') $\|C(m+n,\theta)P(\theta)x\| \leq N(\theta)\|C(n,\theta)P(\theta)x\|$;
(nd_2') $\|C(n,\theta)Q(\theta)x\| \leq N(\theta)\|C(m+n,\theta)Q(\theta)x\|$,

for all $(m, n, \theta, x) \in \mathbb{N}^2 \times \Gamma$.

Definition 3.2. We say that (π, P) is *nonuniformly exponentially dichotomic* if there exist two functions $N, \nu : \Theta \to \mathbb{R}_+^*$ such that:

(ned_1) $\|C(n,\theta)P(\theta)x\| \leq N(\theta)e^{-\nu(\theta)n}\|P(\theta)x\|$;
(ned_2) $e^{\nu(\theta)n}\|Q(\theta)x\| \leq N(\theta)\|C(n,\theta)Q(\theta)x\|$,

for all $(n, \theta, x) \in \mathbb{N} \times \Gamma$.

Remark 3. We observe that, if

- ν is a constant function, then we have the concept of *nonuniform exponential dichotomy in the classical sense*;
- N and ν are constant functions, then obtain the property of *uniform exponential dichotomy*.

Remark 4. The pair (π, P) has a nonuniform exponential dichotomy if and only if there exist $N, \nu : \Theta \to \mathbb{R}_+^*$ with:

(ned_1') $\|C(m+n,\theta)P(\theta)x\| \leq N(\theta)e^{-\nu(\theta)m}\|C(n,\theta)P(\theta)x\|$;
(ned_2') $e^{\nu(\theta)m}\|C(n,\theta)Q(\theta)x\| \leq N(\theta)\|C(m+n,\theta)Q(\theta)x\|$,

for all $(m, n, \theta, x) \in \mathbb{N}^2 \times \Gamma$.

Remark 5. If the pair (π, P) admits nonuniform exponential dichotomy, then (π, P) has nonuniform dichotomy.

Theorem 3.1. *The pair (π, P) is nonuniformly exponentially dichotomic if and only if there exist the functions $\delta,\ \Delta : \Theta \to \mathbb{R}_+^*$ such that the following conditions hold:*

$$(dned_1)\quad \sum_{k=n}^{+\infty} e^{\delta(\theta)k}\|C(k,\theta)P(\theta)x\| \le \Delta(\theta)\|P(\theta)x\|$$

$$(dned_2)\quad \sum_{k=0}^{n} e^{\delta(S(n,\theta))k}\|C(n-k,S(k,\theta))Q(S(k,\theta))x\| \le \Delta(S(n,\theta))\|C(n,S(n,\theta))Q(S(n,\theta))x\|,$$

for all $(n,\theta,x) \in \mathbb{N}\times\Gamma$.

Proof. Necessity. We consider $\delta, \Delta : \Theta \to \mathbb{R}_+^*$, with $\delta(\theta) < \nu(\theta)$ and $\Delta(\theta) = \dfrac{N(\theta)}{1-e^{\delta(\theta)-\nu(\theta)}}$, for all $\theta \in \Theta$. Thus, for all $(n,\theta,x) \in \mathbb{N}\times\Gamma$ we have:

$(dned_1)$

$$\sum_{k=n}^{+\infty} e^{\delta(\theta)k}\|C(k,\theta)P(\theta)x\| \le N(\theta)\sum_{k=0}^{+\infty} e^{\delta(\theta)k}e^{-\nu(\theta)k}\|P(\theta)x\| =$$

$$= N(\theta)\cdot\frac{1}{1-e^{\delta(\theta)-\nu(\theta)}}\|P(\theta)x\| = \Delta(\theta)\|P(\theta)x\|;$$

$(dned_2)$

$$\sum_{k=0}^{n} e^{\delta(S(n,\theta))k}\|Q(S(n,\theta))C(n-k,S(k,\theta))x\| \le$$

$$\le N(S(n,\theta))\sum_{k=0}^{n} e^{(\delta(S(n,\theta))-\nu(S(n,\theta)))k}\|C(k,S(n,\theta))Q(S(n,\theta))C(n-k,S(k,\theta))x\| =$$

$$= N(S(n,\theta))\sum_{k=0}^{n} e^{(\delta(S(n,\theta))-\nu(S(n,\theta)))k}\|C(n,S(n,\theta))Q(S(n,\theta))x\| =$$

$$= N(S(n,\theta))\frac{1-e^{(\delta(S(n,\theta))-\nu(S(n,\theta)))(n+1)}}{1-e^{\delta(S(n,\theta))-\nu(S(n,\theta))}}\|C(n,S(n,\theta))Q(S(n,\theta))x\| \le$$

$$\le \Delta(S(n,\theta))\|C(n,S(n,\theta))Q(S(n,\theta))x\|.$$

Sufficiency. Considering $k = n$ in the relations $(dned_1)$, respectively $(dned_2)$, it follows that

$$e^{\delta(\theta)n}\|C(n,\theta)P(\theta)x\| \le \Delta(\theta)\|P(\theta)x\|,$$

respectively

$$e^{\delta(S(n,\theta))n}\|Q(S(n,\theta))x\| \le \Delta(S(n,\theta))\|C(n,S(n,\theta))Q(S(n,\theta))x\|,$$

for all $(n,\theta,x) \in \mathbb{N}\times\Gamma$, which implies that (π, P) has a nonuniform exponential dichotomy. □

Corollary 3.2. *The pair (π, P) is nonuniformly dichotomic if and only if there are $\delta,\ \Delta : \Theta \to \mathbb{R}_+^*$ such that the conditions $(dned_1)$ and $(dned_2)$ from Theorem 3.1 are verified.*

Proof. It yields from Theorem 3.1 and Remark 5. □

Proposition 1. *Let $P : \Theta \to \mathcal{B}(X)$ be a strongly invariant family of projectors for $\pi = (S, C)$. Then (π, P) is nonuniformly exponentially dichotomic if and only if there are two functions $N, \nu : \Theta \to \mathbb{R}_+^*$ such that:*

(ned_1) $\|C(n,\theta)P(\theta)x\| \leq N(\theta)e^{-\nu(\theta)n}\|P(\theta)x\|$;

(ned_2') $\|D(n,\theta)Q(S(n,\theta))x\| \leq N(\theta)e^{-\nu(\theta)n}\|Q(S(n,\theta))x\|$,

for all $(n, \theta, x) \in \mathbb{N} \times \Gamma$.

Proof. We show that (ned_2') is equivalent with (ned_2), using the relations from Remark 1.
For the implication $(ned_2') \Rightarrow (ned_2)$, we have

$$e^{\nu(\theta)n}\|Q(\theta)x\| = e^{\nu(\theta)n}\|D(n,\theta)C(n,\theta)Q(\theta)x\| =$$

$$= e^{\nu(\theta)n}\|D(n,\theta)Q(S(n,\theta))C(n,\theta)x\| \leq N(\theta)\|Q(S(n,\theta))C(n,\theta)x\| = N(\theta)\|C(n,\theta)Q(\theta)x\|,$$

for all $(n, \theta, x) \in \mathbb{N} \times \Gamma$.
Similarly, for the converse implication $(ned_2) \Rightarrow (ned_2')$, we deduce

$$\|D(n,\theta)Q(S(n,\theta))x\| = \|Q(\theta)D(n,\theta)Q(S(n,\theta))x\| \leq$$

$$\leq N(\theta)e^{-\nu(\theta)n}\|C(n,\theta)Q(\theta)D(n,\theta)Q(S(n,\theta))x\| = N(\theta)e^{-\nu(\theta)n}\|Q(S(n,\theta))x\|,$$

for all $(n, \theta, x) \in \mathbb{N} \times \Gamma$. □

Proposition 2. *Let $P : \Theta \to \mathcal{B}(X)$ be a strongly invariant family of projectors for $\pi = (S, C)$. Then (π, P) admits nonuniform dichotomy if and only if there exists $N : \Theta \to \mathbb{R}_+^*$ such that:*

(nd_1) $\|C(n,\theta)P(\theta)x\| \leq N(\theta)\|P(\theta)x\|$;

(nd_2') $\|D(n,\theta)Q(S(n,\theta))x\| \leq N(\theta)\|Q(S(n,\theta))x\|$,

for all $(n, \theta, x) \in \mathbb{N} \times \Gamma$.

Proof. It is a consequence of Proposition 1. □

Theorem 3.3. *Let $P : \Theta \to \mathcal{B}(X)$ be a strongly invariant family of projectors for $\pi = (S, C)$. The pair (π, P) is nonuniformly exponentially dichotomic if and only if there exist the functions δ, $\Delta : \Theta \to \mathbb{R}_+^*$ such that the following conditions are satisfied:*

$(dned_1)$ $\displaystyle\sum_{k=n}^{+\infty} e^{\delta(\theta)k}\|C(k,\theta)P(\theta)x\| \leq \Delta(\theta)\|P(\theta)x\|$

$(dned_2')$ $\displaystyle\sum_{k=0}^{n} e^{\delta(\theta)(n-k)}\|D(n-k,S(k,\theta))Q(S(n,\theta))x\| \leq \Delta(\theta)\|Q(S(n,\theta))x\|$,

for all $(n, \theta, x) \in \mathbb{N} \times \Gamma$.

Proof. Necessity. We consider $\delta, \Delta : \Theta \to \mathbb{R}_+^*$, with $\delta(\theta) < \nu(\theta)$ and $\Delta(\theta) = \dfrac{N(\theta)}{1 - e^{\delta(\theta)-\nu(\theta)}}$, for all $\theta \in \Theta$.
The condition $(dned_1)$ follows as in Theorem 3.1.

For $(dned_2')$ we use Proposition 1 and we obtain

$$\sum_{k=0}^{n} e^{\delta(\theta)(n-k)}\|D(n-k,S(k,\theta))Q(S(n,\theta))x\| \leq N(\theta)\sum_{k=0}^{n} e^{(\delta(\theta)-\nu(\theta))(n-k)}\|Q(S(n,\theta))x\| \leq$$

$$\leq N(\theta)\frac{e^{\nu(\theta)-\delta(\theta)}-e^{(\delta(\theta)-\nu(\theta))n}}{e^{\nu(\theta)-\delta(\theta)}-1}\|Q(S(n,\theta))x\| \leq \Delta(\theta)\|Q(S(n,\theta))x\|,$$

for all $(n,\theta,x)\in\mathbb{N}\times\Gamma$.

Sufficiency. Taking $k=n$ in the relation $(dned_1)$, it results

$$e^{\delta(\theta)n}\|C(n,\theta)P(\theta)x\| \leq \Delta(\theta)\|P(\theta)x\|$$

and for $k=0$ in $(dned_2')$ we deduce

$$e^{\delta(\theta)n}\|D(n,\theta)Q(S(n,\theta))x\| \leq \Delta(\theta)\|Q(S(n,\theta))x\|,$$

for all $(n,\theta,x)\in\mathbb{N}\times\Gamma$.
Hence, (π,P) is nonuniformly exponentially dichotomic. □

Corollary 3.4. *The pair (π,P) admits a nonuniform dichotomy if and only if there are δ, $\Delta:\Theta\to\mathbb{R}_+^*$ such that the conditions $(dned_1)$ and $(dned_2')$ from Theorem 3.3 hold.*

Proof. It follows from Theorem 3.3 and Remark 5. □

References

Alonso, A. I., J. Hong and R. Obaya (1999). Exponential dichotomy and trichotomy for difference equations. *Comp. Math. Appl.* **38**, 41–49.

Babuţia, M. G. and M. Megan (2016). Nonuniform exponential dichotomy for discrete dynamical systems in Banach spaces. *Mediterr. J. Math.* **13**, 1653–1667.

Biriş, L. and M. Megan (2016). On a concept of exponential dichotomy for cocycles of linear operators in Banach spaces. *Bull. Math. Soc. Sci. Math. Roumanie* **59(107)**(3), 217–223.

Biriş, L. E., T. Ceauşu and C. L. Mihiţ (2019). On uniform exponential splitting of variational nonautonomous difference equations in Banach spaces. In: *Springer Proceedings in Mathematics & Statistics, Recent Progress in Difference Equations, Discrete Dynamical Systems and Applications (to appear), ISBN 978-3-030-20015-2*.

Chow, S. N. and H. Leiva (1996). Two definitions of exponential dichotomy for skew-product semiflows in Banach spaces. *Proc. Amer. Math. Sc.* **124**, 1071–1081.

Crai, V. (2016). On the robustness of a concept of dichotomy with different growth rates for linear discrete-time systems in Banach spaces. In: *Proceedings of 11th IEEE International Symposium on Applied Computational Intelligence and Informatics*. pp. 123–130.

Elaydi, S. and K. Janglajew (1998). Dichotomy and trichotomy of difference equations. *J. Difference Equ. Appl.* **3**, 417–448.

Huy, N. T. and H. Phi (2010). Discretized characterizations of exponential dichotomy of linear skew-product semiflows over semiflows. *J. Math. Anal. Appl.* **362**, 46–57.

Megan, M. and C. Stoica (2010). Concepts of dichotomy for skew-evolution semiflows in Banach spaces. *Ann. Acad. Rom. Sci. Ser. Math. Appl.* **2**(2), 125–140.

Megan, M., B. Sasu and A. L. Sasu (2002). On nonuniform exponential dichotomy of evolution operators in Banach spaces. *Integral Equations Operator Theory* **44**, 71–78.

Popa, I. L., M. Megan and T. Ceauşu (2012). Exponential dichotomies for linear discrete-time systems in Banach spaces. *Appl. Anal. Discrete Math.* **6**, 140–155.

Przyluski, K. M. and S. Rolewicz (1984). On stability of linear time-varying infinite-dimensional discrete-time systems. *Systems & Control Letters* **4**(5), 307–315.

Sasu, B. (2009). On exponential dichotomy of variational difference equations. *Discrete Dyn. Nat. Soc.* **2009**(Article ID 324273), 18 pages.

Sasu, B. and A. L. Sasu (2013). On the dichotomic behavior of discrete dynamical systems on the half-line. *Discrete Contin. Dyn. Syst.* **33**(7), 3057–3084.

Stoica, C. (2016). Approaching the discrete dynamical systems by means of skew-evolution semiflows. *Discrete Dyn. Nat. Soc.* **2016**(Article ID 4375069), 10 pages.

Theory and Applications of Mathematics & Computer Science

(ISSN 2067-2764, EISSN 2247-6202)
http://www.uav.ro/applications/se/journal/index.php/tamcs

Theory and Applications of Mathematics & Computer Science 9 (1) (2019) 8 – 13

Polynomial Stability in Average for Cocycles of Linear Operators

Rovana Boruga (Toma)[a,*]

[a]*West University of Timişoara, Faculty of Mathematics and Computer Science, Department of Mathematics, Bd. V. Pârvan 4, RO-300223 Timişoara, Romania.*

Abstract

In the present paper we deal with the concept of polynomial stability in average. We obtain two characterization theorems that describe the concept mentioned above. In fact, we give a logarithmic criterion and a Datko type theorem for cocycles of linear operators.

Keywords: cocycles of linear operators, polynomial stability in average
2010 MSC: 34D05, 34D20 .

1. Introduction

The notion of exponential dichotomy in average was introduced by L.Barreira, D.Dragicevic and C. Valls in (Barreira *et al.*, 2016) and it includes the classical concept of uniform exponential dichotomy which appeared due to Perron (Perron, 1930).

A particular case of this dichotomy behavior was studied by Dragicevic in (Dragicevic, 2016). He obtained a version of a well known theorem of R. Datko for the notion of the exponential stability in average for cocycles over flows and also for cocycles over maps.

In (Hai, 2019) the author uses the theory of Banach function spaces to characterize polynomially bounded stochastic skew evolution semiflows. He talks about polynomial stability and polynomial instability in mean. He states and proves results which are continuous or discrete-time versions of the Datko type characterization theorems.

The objective of this paper is to find for cocycles of linear operators, similar approaches as in the exponential case, for the classical polynomial stability concept, that has been studied in many papers (Barreira & Valls, 2009), (Hai, 2015), (Megan *et al.*, 2003). In fact, we consider cocycles acting on functions from L^1 and we give a version of a logarithmic criterion for the concept of polynomial stability in average which is similar to the one obtained for the classical uniform polynomial stability concept. Also, we prove a Datko type characterization theorem for the concept mentioned.

*Corresponding author
Email address: rovanaboruga@gmail.com (Rovana Boruga (Toma))

2. Preliminaries

Let $(\Omega, \mathrm{B}, \mu)$ be a probability space. We consider the sets $\Delta = \{(t, s) \in \mathbb{R}_+^2 : t \geq s\}$ and $T = \{(t, s, t_0) \in \mathbb{R}_+^3 : t \geq s \geq t_0\}$.

Definition 2.1. An application $\varphi : \mathbb{R}_+ \times \Omega \to \Omega$ is called a semiflow on Ω if:

(s_1) $\varphi(0, \omega) = \omega$, for all $\omega \in \Omega$.

(s_2) $\varphi(t + s, \omega) = \varphi(t, \varphi(s, \omega))$, for all $(t, s, \omega) \in \Delta \times \Omega$.

Let X be a Banach space and $\mathrm{B}(X)$ the Banach algebra of all bounded linear operators acting on X.

Definition 2.2. An application $\Phi : \mathbb{R}_+ \times \Omega \to \mathrm{B}(X)$ is called a cocycle over the semiflow φ if:

(c_1) $\forall x \in X$ the mapping $(t, \omega) \mapsto \Phi(t, \omega)x$ is Bochner measurable.

(c_2) $\forall (t, \omega) \in \mathbb{R}_+ \times \Omega,\ \exists\, \Phi(t, \omega)^{-1}$.

(c_3) $\Phi(0, \omega) = I, \forall \omega \in \Omega$, where I is the identity operator on X.

(c_4) $\Phi(t + s, \omega) = \Phi(t, \varphi(s, \omega))\, \Phi(s, \omega), \forall t, s \geq 0, \forall \omega \in \Omega$.

Let $L^1(\Omega, X, \mu)$ be the Banach space of all Bochner measurable functions $x : \Omega \to X$ such that

$$\|x\|_1 := \int_\Omega \|x(\omega)\|\, d\mu(\omega) < \infty.$$

In what follows, we will denote by

$$\Phi_\omega(t, s) = \Phi(t, \omega)\, \Phi(s, \omega)^{-1}, \forall t, s \geq 0, \forall \omega \in \Omega.$$

Remark 2.1. It is easy to see that an evolution property holds:

$$\Phi_\omega(t, t_0) = \Phi_\omega(t, s)\, \Phi_\omega(s, t_0),\ \forall t \geq s \geq t_0 \geq 0,\ \forall \omega \in \Omega.$$

Indeed, $\Phi_\omega(t, s)\, \Phi_\omega(s, t_0) = \Phi(t, \omega)\, \Phi(s, \omega)^{-1}\, \Phi(s, \omega)\, \Phi(t_0, \omega)^{-1} = \Phi(t, \omega)\, \Phi(t_0, \omega)^{-1} = \Phi_\omega(t, t_0)$.

3. Polynomial stability in average

Definition 3.1. The cocycle $\Phi : \mathbb{R}_+ \times \Omega \to \mathrm{B}(X)$ is polynomially stable in average if there exist $N > 1$ and $\nu > 0$ such that

$$\int_\Omega \|\Phi_\omega(t, s)x(\omega)\| d\mu(\omega) \leq M \left(\frac{s+1}{t+1}\right)^\nu \int_\Omega \|x(\omega)\|\, d\mu(\omega)$$

for all $(t, s, \omega) \in \Delta \times \Omega$.

Remark 3.1. The cocycle $\Phi : \mathbb{R}_+ \times \Omega \to \mathrm{B}(X)$ is polynomially stable in average if and only if there exist $N > 1$ and $\nu > 0$ such that

$$\int_\Omega \|\Phi_\omega(t, t_0)x(\omega)\| d\mu(\omega) \leq N \left(\frac{s+1}{t+1}\right)^\nu \int_\Omega \|\Phi_\omega(s, t_0)x(\omega)\|\, d\mu(\omega)$$

for all $(t, s, t_0, \omega) \in T \times \Omega$.

Definition 3.2. The cocycle $\Phi : \mathbb{R}_+ \times \Omega \to \mathrm{B}(X)$ is uniformly stable in average if there exists $N > 1$ such that

$$\int_{\Omega} \|\Phi_\omega(t, s)x(\omega)\| d\mu(\omega) \leq N \int_{\Omega} \|x(\omega)\| \, d\mu(\omega)$$

for all $(t, s, \omega) \in \Delta \times \Omega$.

Remark 3.2. The cocycle $\Phi : \mathbb{R}_+ \times \Omega \to \mathrm{B}(X)$ is uniformly stable in average if and only if there exist $N > 1$ such that

$$\int_{\Omega} \|\Phi_\omega(t, t_0)x(\omega)\| d\mu(\omega) \leq N \int_{\Omega} \|\Phi_\omega(s, t_0)x(\omega)\| \, d\mu(\omega)$$

for all $(t, s, t_0, \omega) \in T \times \Omega$.

Definition 3.3. The cocycle $\Phi : \mathbb{R}_+ \times \Omega \to \mathrm{B}(X)$ has polynomial growth in average if there exist $M > 1$ and $\alpha > 0$ such that

$$\int_{\Omega} \|\Phi_\omega(t, s)x(\omega)\| d\mu(\omega) \leq M \left(\frac{t+1}{s+1}\right)^{\alpha} \int_{\Omega} \|x(\omega)\| \, d\mu(\omega)$$

for all $(t, s, \omega) \in \Delta \times \Omega$.

Remark 3.3. The cocycle $\Phi : \mathbb{R}_+ \times \Omega \to \mathrm{B}(X)$ has polynomial growth in average if and only if there exist $M > 1$ and $\alpha > 0$ such that

$$\int_{\Omega} \|\Phi_\omega(t, t_0)x(\omega)\| d\mu(\omega) \leq M \left(\frac{t+1}{s+1}\right)^{\alpha} \int_{\Omega} \|\Phi_\omega(s, t_0)x(\omega)\| \, d\mu(\omega)$$

for all $(t, s, t_0\omega) \in T \times \Omega$.

In what follows, we will present a logarithmic criterion for the concept of polynomial stability in average.

Theorem 3.1. *Let Φ be a cocycle with polynomial growth in average. Then Φ in polynomially stable in average if and only if there exist a constant $L > 1$ such that:*

$$\int_{\Omega} \|\Phi_\omega(t, s)x(\omega)\| d\mu(\omega) \ln \frac{t+1}{s+1} \leq L \int_{\Omega} \|x(\omega)\| \, d\mu(\omega)$$

for all $t, s \geq 1, \omega \in \Omega$.

Proof. Necessity. We suppose that Φ is polynomially stable in average. Then, there exist $N \geq 1$ and $\nu > 0$ such that

$$\int_{\Omega} \|\Phi_\omega(t, s)x(\omega)\| d\mu(\omega) \ln \frac{t+1}{s+1} \leq N \left(\frac{t+1}{s+1}\right)^{-\nu} \ln \frac{t+1}{s+1} \int_{\Omega} \|x(\omega)\| d\mu(\omega).$$

We consider the application $f : [1, \infty) \to \mathbb{R}$, $f(u) = u^{-\nu} \ln u$, where $u = \dfrac{t+1}{s+1}$. Then, we obtain $f(u) \leq \dfrac{N}{\nu e}$. It results that

$$\int_{\Omega} \|\Phi_\omega(t, s)x(\omega)\| d\mu(\omega) \ln \frac{t+1}{s+1} \leq L \int_{\Omega} \|x(\omega)\| d\mu(\omega), \text{ where } L = 1 + \frac{N^2}{\nu e}.$$

Sufficiency. We denote by $S = \sup_{t\geq s\geq 1} \int_\Omega \|\Phi_\omega(t,s)x(\omega)\|\, d\mu(\omega) \ln\frac{t+1}{s+1}$.

Step 1. Let $n \overset{d}{=} \left[\frac{\ln\left(\frac{t}{s}\right)}{4S}\right]$, with $(t,s)\in\Delta$, $s\geq 1$. Then, the following inequalities hold:

(1) $se^{4nS} \leq t < se^{4(n+1)S}$

(2) $\left(\frac{t+1}{s+1}\right)^{\frac{\ln 2}{4S}} \leq 2^{n+1}$, for all $t\geq s\geq 1$.

Indeed, the first relation is a simple computation which uses the property of the whole part of a number and the second inequality results immediately from the first one.

Step 2. We prove that

$$\int_\Omega \|\Phi_\omega(se^{4S},s)x(\omega)\|\, d\mu(\omega) \leq \frac{1}{2}\int_\Omega \|x(\omega)\|\, d\mu(\omega),\ \forall s\geq 1, \forall\omega\in\Omega$$

From $\frac{1+s^{4S}}{1+s} \geq e^{2S}$, it results that

$$\int_\Omega \|\Phi_\omega(se^{4S},s)x(\omega)\|\, d\mu(\omega) \leq \frac{S}{\ln\frac{1+se^{4S}}{1+s}}\int_\Omega \|x(\omega)\|\, d\mu(\omega) \leq \frac{S}{\ln e^{2S}}\int_\Omega \|x(\omega)\| d\mu(\omega) = \frac{1}{2}\int_\Omega \|x(\omega)\|\, d\mu(\omega).$$

Step 3. We show that

$$\int_\Omega \|\Phi_\omega(se^{4nS},s)x(\omega)\|\, d\mu(\omega) \leq \frac{1}{2^n}\int_\Omega \|x(\omega)\| d\mu(\omega), \forall s\geq 1, \forall\omega\in\Omega.$$

Indeed, using step 2, we have

$$\begin{aligned}\int_\Omega \|\Phi_\omega(se^{4nS},s)x(\omega)\|\, d\mu(\omega) &= \int_\Omega \|\Phi_\omega(se^{4nS},se^{4(n-1)S})\Phi(se^{4(n-1)S},s)\|x(\omega)\|\, d\mu(\omega) \leq \\ &\leq \frac{1}{2}\int_\Omega \|\Phi_\omega(se^{4(n-1)S},s)x(\omega)\|\, d\mu(\omega) \leq \cdots \leq \frac{1}{2^n}\int_\Omega \|x(\omega)\| d\mu(\omega).\end{aligned}$$

Step 4. We prove that Φ is polynomially stable in average using the evolution property proved in Remark [2.1] and the previous steps.

$$\begin{aligned}\int_\Omega \|\Phi_\omega(t,s)x(\omega)\| d\mu(\omega) &= \int_\Omega \|\Phi_\omega(t,se^{4nS})\cdot\Phi_\omega(se^{4nS},s)x(\omega)\| d\mu(\omega) \leq \\ &\leq M\left(\frac{1+t}{1+se^{4nS}}\right)^\alpha \cdot \frac{1}{2^n}\int_\Omega \|x(\omega)\| d\mu(\omega) \leq \frac{Me^{4\alpha S}}{2^n}\int_\Omega \|x(\omega)\| d\mu(\omega) \leq \\ &\leq 2Me^{4\alpha S}\left(\frac{t+1}{s+1}\right)^{\frac{-\ln 2}{4S}}\int_\Omega \|x(\omega)\| d\mu(\omega) \leq N\left(\frac{t+1}{s+1}\right)^{-\nu}\int_\Omega \|x(\omega)\| d\mu(\omega),\end{aligned}$$

where $N = 2Me^{4\omega S} > 1$ and $\nu = \dfrac{\ln 2}{4S} > 0$.

□

Next, we will give a Datko type theorem for the polynomial stability in average concept.

Theorem 3.2. *Let Φ be a cocycle with polynomial growth in average. Then Φ is polynomially stable in average if and only if there exist the constants $D > 1$ and $d \geq 0$ such that*

$$\int_s^\infty (\tau+1)^{d-1}\left(\int_\Omega \|\Phi_\omega(\tau,s)x(\omega)\|\, d\mu(\omega)\right)d\tau \leq D(s+1)^d \int_\Omega \|x(\omega)\|\, d\mu(\omega), \forall s \geq 0, \forall \omega \in \Omega. \tag{3.1}$$

Proof. Neccesity. We suppose that Φ is polynomially stable in average. Then, we have that there exist $N \geq 1, \nu > 0$ such that for all $d \in [0, \nu)$:

$$\int_s^\infty (\tau+1)^{d-1}\left(\int_\Omega \|\Phi_\omega(\tau,s)x(\omega)\|\, d\mu(\omega)\right)d\tau \leq N\int_s^\infty (\tau+1)^{d-1}\left(\frac{s+1}{\tau+1}\right)^\nu \int_\Omega \|x(\omega)\|\, d\mu(\omega)d\tau =$$

$$= N(s+1)^\nu \int_\Omega \|x(\omega)\|\, d\mu(\omega)\int_s^\infty (\tau+1)^{d-\nu-1}d\tau = \frac{N}{\nu-d}(s+1)^d \int_\Omega \|x(\omega)\|\, d\mu(\omega) \leq$$

$$\leq D(s+1)^d \int_\Omega \|x(\omega)\|\, d\mu(\omega), \text{ where } D = 1 + \frac{N}{\nu-d}.$$

Sufficiency. We suppose that there exist $D > 1$ and $d \geq 0$ such that the integral inequality form the theorem states. First, we discuss the case when $d > 0$.
If $t \geq 2s+1$ we have

$$(t+1)^d \int_\Omega \|\Phi_\omega(t,s)x(\omega)\|\, d\mu(\omega) = \frac{2}{t+1}\int_{\frac{t-1}{2}}^t (t+1)^d \cdot \int_\Omega \|\Phi_\omega(t,s)x(\omega)\|\, d\mu(\omega)d\tau \leq$$

$$\leq 2\int_{\frac{t-1}{2}}^t \frac{(t+1)^d}{\tau+1}\int_\Omega \|\Phi_\omega(t,\tau)\Phi_\omega(\tau,s)x(\omega)\|\, d\mu(\omega)d\tau \leq 2M\int_{\frac{t-1}{2}}^t \frac{(t+1)^d}{\tau+1}\left(\frac{t+1}{\tau+1}\right)^{d+\alpha}\int_\Omega \|\Phi_\omega(\tau,s)x(\omega)\|\, d\mu(\omega)d\tau \leq$$

$$\leq 2^{\alpha+d+1}\cdot M\int_s^\infty (\tau+1)^{d-1}\int_\Omega \|\Phi_\omega(\tau,s)x(\omega)\|\, d\mu(\omega)d\tau \leq N_1(s+1)^d\int_\Omega \|x(\omega)\|\, d\mu(\omega)d\tau.$$

If $t \in [s, 2s+1)$, we obtain that $\dfrac{t+1}{s+1} \leq 2$. Then using the growth property we obtain

$$(t+1)^d \int_\Omega \|\Phi_\omega(t,s)x(\omega)\|\, d\mu(\omega) \leq (t+1)^d M\left(\frac{t+1}{s+1}\right)^\alpha \int_\Omega \|x(\omega)\|\, d\mu(\omega) \leq N_2(s+1)^d \int_\Omega \|x(\omega)\|\, d\mu(\omega).$$

So, it results that Φ is polynomially stable in average. Next, we deal with the case when $d = 0$. From (3.2), for $d = 0$ it results

$$\int_s^\infty \frac{1}{\tau+1}\left(\int_\Omega \|\Phi_\omega(\tau,t_0)x(\omega)\|\, d\mu(\omega)\right)d\tau \le D\int_\Omega \|\Phi_\omega(s,t_0)x(\omega)\|\, d\mu(\omega), \forall (s,t_0)\in\Delta, \forall\omega\in\Omega.$$

Step 1. We prove that Φ is uniformly stable in average. Indeed, we consider firstly $t \ge 2s+1$ and then $t \in [s, 2s+1)$ and using similar techniques as in the first case we obtain the conclusion.

Step 2. We show that Φ is polynomially stable in average using the logarithmic criterion.

$$\int_\Omega \|\Phi_\omega(t,s)x(\omega)\|\, d\mu(\omega)\ln\frac{t+1}{s+1} = \int_s^t \frac{1}{\tau+1}\int_\Omega \|\Phi_\omega(t,s)x(\omega)\|\, d\mu(\omega)d\tau \le \int_s^\infty \frac{1}{\tau+1}\int_\Omega \|\Phi_\omega(t,s)x(\omega)\|\, d\mu(\omega)d\tau \le$$
$$\le D\int_\Omega \|x(\omega)\|\, d\mu(\omega)$$

From Theorem [3.1] it results that the cocycle Φ is polynomially stable in average. □

References

Barreira, L. and C. Valls (2009). Polynomial growth rates. *Nonlinear Analysis* **7**, 5208–5219.

Barreira, L., D. Dragicevic and C. Valls (2016). Exponential dichotomies in average for flows and admissibility. *Publ. Math. Debrecen*.

Dragicevic, D. (2016). A version of a theorem of R. Datko for stability in average. *Systems and Control Letters* **96**, 1–6.

Hai, P.V. (2015). On the polynomial stability of evolution families. *Applicable Analysis* **95**(6), 1239–1255.

Hai, P.V. (2019). Polynomial behavior in mean of stochastic skew-evolution semiflows. *arXiv:1902.04214v1 [math.PR]*.

Megan, M., A. L. Sasu and B. Sasu (2003). *The Asymptotic Behavior of Evolution Families*. Mirton Publishing House.

Perron, O. (1930). Die stabilitätsfrage bei differentialgleichungen. *Math. Z.* **32**, 703–728.

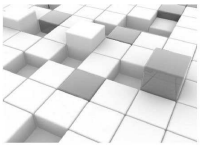

Theory and Applications of Mathematics & Computer Science

(ISSN 2067-2764, EISSN 2247-6202)
http://www.uav.ro/applications/se/journal/index.php/tamcs

Theory and Applications of Mathematics & Computer Science 9 (1) (2019) 14 – 27

Ghrist Barcoded Video Frames. Application in Detecting Persistent Visual Scene Surface Shapes captured in Videos

Arjuna P.H. Don[a], James F. Peters[a,b,*]

[a] *Computational Intelligence Laboratory, University of Manitoba, WPG, MB, R3T 5V6, Canada*
[b] *Department of Mathematics, Faculty of Arts and Sciences, Adıyaman University, 02040, Adıyaman, Turkey.*

Abstract

This article introduces an application of Ghrist barcodes in the study of persistent Betti numbers derived from vortex nerve complexes found in triangulations of video frames. A Ghrist barcode (also called a persistence barcode) is a topology of data pictograph useful in representing the persistence of the features of changing shapes. The basic approach is to introduce a free Abelian group representation of intersecting filled polygons on the barycenters of the triangles of Alexandroff nerves. An Alexandroff nerve is a maximal collection of triangles of a common vertex in the triangulation of a finite, bounded planar region. In our case, the planar region is a video frame. A Betti number is a count of the number of generators is a finite Abelian group. The focus here is on the persistent Betti numbers across sequences of triangulated video frames. Each Betti number is mapped to an entry in a Ghrist barcode. Two main results are given, namely, vortex nerves are Edelsbrunner-Harer nerve complexes and the Betti number of a vortex nerve equals $k + 2$ for a vortex nerve containing k edges attached between a pair of vortex cycles in the nerve.

Keywords: Betti Number, Ghrist barcode, Hole, Topology of Data, Vortex Nerve, Video Frame Shape
2010 MSC No: Primary 55N99 (Persistent Homology), Secondary 68U05 (Computational Geometry).

1. Introduction

This paper introduces an application of Ghrist barcodes in classifying and identifying persistent video frame shapes. This approach to video frame shape detection and analysis provides a foundation for machine learning in the study of persistent video frame shapes and a vidoe-shrinking approach to solving the big data problem relative to videos containing thousands of redundant frames.

A **Ghrist barcode**, usually called a **persistence barcode**, is a topology-of-data pictograph that represents that appearance and disappearance of consecutive sequences of video frames having a particular feature value (Ghrist, 2008), (Ghrist, 2014, §5.13, pp. 104-106). The origin of topology-of-data

*Corresponding author: 75A Chancellor's Circle, EITC-E2-390, University of Manitoba, WPG, MB R3T 5V6, Canada; e-mail: james.peters3@ad.umanitoba.ca, research has been supported by the Natural Sciences & Engineering Research Council of Canada (NSERC) discovery grant 185986, Instituto Nazionale di Alta Matematica (INdAM) Francesco Severi, Gruppo Nazionale per le Strutture Algebriche, Geometriche e Loro Applicazioni grant 9 920160 000362, n.prot U 2016/000036 and Scientific and Technological Research Council of Turkey (TÜBİTAK) Scientific Human Resources Development (BIDEB) under grant no: 2221-1059B211301223.

Email addresses: pilippua@myumanitoba.ca (Arjuna P.H. Don), James.Peters3@umanitoba.ca (James F. Peters)

barcodes can be traced back to H. Edelsbrunner, D. Letscher and A. Zomorodian (Edelsbrunner *et al.*, 2000), (Edelsbrunner *et al.*, 2001). For a complete view of the landscape for a topology-of-data barcode viewed as a multiset of intervals[1], see J.A. Perea (Perea, 2018). In this paper, the Betti number of a triangulated video frame vortex nerve is represented by consecutive sequences of frames with holes (gaps) between them. A *vortex nerve* is a collection of nesting, possibly overlapping filled vortexes attached to each other and have nonempty intersection (Ahmad & Peters, 2018; Peters & Ramanna, 2018; Peters, 2018*b*,*a*, 2017). A *filled vortex* has a boundary that is a simple closed curve and a nonempty interior.

Each of the vertices on the edges of a vortex nerve is a barycenter (intersection of triangle median lines) in a triangle in an Alexandroff nerve, introduced by P. Alexandroff [Aleksandrov] (Alexandroff, 1965, §31, p. 39), (Alexandroff, 1926) and elaborated in (Alexandrov, 1956, Vol. 3, p. 67), (Alexandroff & Hopf, 1935, §2.11, pp. 160-161). Briefly, an *Alexandroff nerve* is a collection of triangles with a common vertex. Each vortex in a nerve has a corresponding cyclic group with a generating element and a Betti number equal to 1. The *Betti number* of a vortex nerve is a count of the number of generating elements in the nerve. A Ghrist barcode that records the multiple occurences of video frames containing a vortex nerve with Betti number equal to 8 is shown in Fig. 1. Each row of the video Ghrist barcode in Fig. 1 represents a sequence of frames containing vortex nerves with the same Betti number.

Vortex nerves in triangulated video frames are of important in this work, since the edges and interior each vortex nerve reveal paths of reflected light between video frame dark regions (image holes). Because of their very simple structure, it is a straightforward task to compute the Betti number of a vortex nerve and equally straightforward task to derive a Betti-number based barcode for each triangulated video. For a particular Betti number, it is common to find sequences of video frames separated by gaps (frames with a different Betti number) in an entire video.

This observation leads to the production of focused (reduced) videos containing only video frames with a particular video number. Here, the basic approach, inspired by B. Le, H. Nguyen and D. Tran (Le *et al.*, 2014), is to shrink a video so that only frames with a recurrent vortex nerve Betti number of interest are retained in a video. Video shrinking (*i.e.*, video frame elimination) is achieved by deleting those frames represented by gaps between occurrences of frames that yield consecutive sequences of a particular vortex nerve Betti number.

The end result of this approach is easy as well quick access to triangulated video frames that represent a particular Betti number. The beneficial side-effect of reduced videos is the focus on the minute changes in persistent surface shapes recorded in sequences of frames with a single Betti number orientation.

2. Preliminaries

This section briefly introduces the methods used to derive vortex nerves and their Betti numbers as well as the method used to construct the Ghrist barcode for a video. The sample barcode in Fig. 1 is the result of the following steps leading from the detection of a vortex nerve in each triangulated video frame to the Betti number representing the video frame, *i.e.*,

Steps leading to a Ghrist barcode entry for video frame Betti number:

Step 1 **Select a video** v, a sequence of frames $fr[1], \ldots, \boldsymbol{fr[i]}, \ldots, fr[n]$.
Step 2 **Select** i^{th} **frame** $fr[i]$ in video v.

[1]Many thanks to Vidit Nanda for pointing this out.

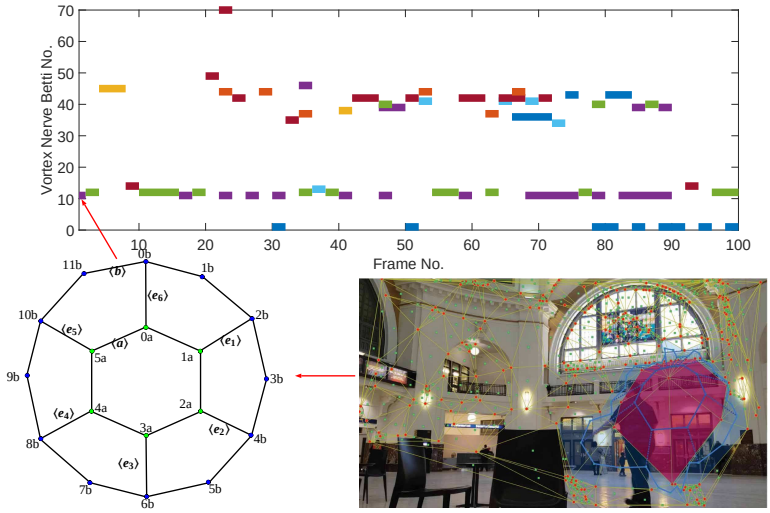

Figure 1. Video barcode entry derived from a triangulated frame with vortex nerve Betti no. = 8

Step 3 **Frame** $fr[i]$ **frame** maps to a set of centroids S on image holes (black regions in a binary image).
Step 4 **Frame Centroids** S map to a set of nonoverlapping triangles $\{\triangle\}$.
Step 5 **Triangles** $\{\triangle\}$ map to a set of barycenters B.
Step 6 **Barycenters** B map to a vortex nerve $\mathrm{sk}_{\mathrm{cyclic}}\mathrm{Nrv}E$.
Step 7 **Vortex nerve** $\mathbf{sk}_{\mathbf{cyclic}}\mathbf{Nrv}E$ maps to Betti number $\mathcal{B}(\mathrm{sk}_{\mathrm{cyclic}}\mathrm{Nrv}E)$, which is a count of the number of overlapping vortexes plus the number of edges (called cusp filaments) connected between the vortexes.
Step 8 **Betti number** $\boldsymbol{\mathcal{B}(\mathbf{sk}_{\mathbf{cyclic}}\mathbf{Nrv}E)}$ maps to an entry (tiny bar) in a row of a video Ghrist barcode.

$$fr[i] \longrightarrow \boxed{S} \longrightarrow \boxed{\{\triangle\}} \longrightarrow \boxed{B} \longrightarrow \boxed{\mathrm{sk}_{\mathrm{cyclic}}\mathrm{Nrv}\boldsymbol{E}} \longrightarrow \boldsymbol{\mathcal{B}}(\mathrm{sk}_{\mathrm{cyclic}}\mathrm{Nrv}\boldsymbol{E})$$

Figure 2. Stages from video frame $fr[i]$ to Betti no. $\mathcal{B}(\mathrm{sk}_{\mathrm{cyclic}}\mathrm{Nrv}E)$ of vortex nerve $\mathrm{sk}_{\mathrm{cyclic}}\mathrm{Nrv}E$

The mappings in steps 3 to 7 are shown in Fig. 2. Each mapping in these steps establishes a correspondence between an object such as the set of centroids S

Example 1. Mapping of a Frame Betti number to a Video Ghrist Barcode Entry.
An illustration of the steps leading to a video Ghrist barcode entry is partially represented in Fig. 1. In this case, a vortex nerve with Betti number equal to 8 is derived from a sample video frame. In Fig. 1, the barycenters of the triangles on the sample video frame are mapped to a vortex nerve (step 6) $sk_{cyclic}NrvE$. *The Betti number of the nerve* $sk_{cyclic}NrvE$ *is mapped to a tiny bar entry in a row of the Ghrist barcode (step 8).* ■

2.1. Holes, geometric centroids, triangulation, barycenters and vortexes

A *hole* is a surface retion that absorbs light. In terms of optical sensors that record the intensity and colour of light reflected from visual scene surfaces, near zero intensities correspond to dark (hole) surface regions. In the morphology of binary images, each centroid is the center of mass of a dark image region that corresponds to a visual scene surface hole. Let X be a set of points in an n-sided filled polygonal 2D region (called a

homogeneous plate) containing vertices with coordinates $(x_i, y_i), i = 1, \ldots, n$ in the Euclidean plane. Then, for example, the coordinates x_c, y_c of the geometric centroid in a 2D homogeneous plate are

$$x_c = \frac{1}{n}\sum_{i=1}^{n} x_i, y_c = \frac{1}{n}\sum_{i=1}^{n} y_i.$$

For more about centroids, see M. Berger (Berger, 1994, §3.4.2, pp. 76-77) (see, also, T. Apostol and M.A. Mnatsakanian (Apostol & Mnatsakanian, 2000)).

Algorithm 1: Filled Delaunay Triangle Construction

Input : Set of centroids S on the holes (dark regions) on video frame
Output: Delaunay Triangle Construction

1 *Let p be a centroid in S;*
2 **Triangle Vertexes Selection Step***; Select centroids $q, r \in S$ nearest $p \in S$;*
3 *Draw edge $\widehat{pq}$ on a closed half plane π_{pq} that covers $r \in S$;*
4 *Draw edge $\widehat{pr}$ on a closed half plane π_{pr} that covers $q \in S$;*
5 *Draw edge $\widehat{qr}$ on a closed half plane π_{qr} that covers $p \in S$;*
6 *Edges on triangle $\triangle(pqr)$ are on intersecting half planes covering $\triangle(pqr)$;*
7 /* $\triangle(pqr)$ is a filled Delaunay triangle */ ;

A centroid is also called a seed point, which is used as a vertex in the triangulation of a digital image. By selecting a set of seed points that are image centroids, it is then possible to construct a collection of what are known as Delaunay triangles on the image. Let p, q, r be three neighbouring image centroids is a set of seed points S and let $\pi_{pq}, \pi_{pr}, \pi_{qr}$ be three half planes. Then Alg. 1 is used to construct a filled Delaunay triangle.

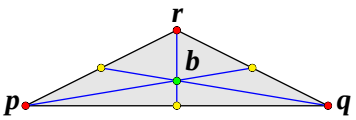

Figure 3. Filled Delaunay triangle $\triangle(pqr)$ barycenter b

The intersection of the median lines of a filled Delaunay triangle is *barycenter* of the triangle.

Example 2. Sample Barycenters of Filled Dalaunay Triangles.
Let $\triangle(pqr)$ be a filled Delaunay triangle as shown in Fig. 3. The median line *of a triangle is the line drawn from a triangle vertex to the midpoint of the side opposite the vertex. Three median lines are also shown in Fig. 3. The barycenter of $\triangle(pqr)$ is located at the intersection of the median lines (shown with a green • in Fig. 3). Many other examples of Delaunay triangle barycenters are shown in Fig. 7.* ■

The important thing to notice here is that an image barycenter on a centroidal triangle is in an image region between the dark regions (holes) in a visual scene. In other words, the barycenter of a centroidal triangle like $\triangle(pqr)$ in Fig. 3 originates from a surface shape that reflects or refracts light bombarding the surface.

Alexandroff Nerve Triangles ⟼ Barycentric Vortex Cycle:
The next step is to select an Alexandroff nerve Nrv$E$ (*i.e.*, collection of triangles with a common vertex).

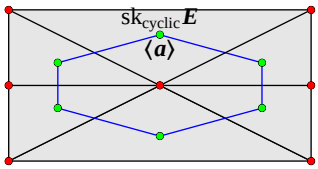

Figure 4. Barycentric vortex cycle $\mathrm{sk}_{\mathrm{cyclic}}\boldsymbol{E}$ with generator $\langle \boldsymbol{a} \rangle$ on an Alexandroff nerve

Next, locate the barycenters of the triangles in Nrv$E$. Then draw edges of half planes between neighbouring barycenters on nerve Nrv$E$. Each barycentric half plane covers the nucleus (common vertex) of Nrv$E$. The end result is a filled *vortex cycle E* (denoted by $\mathrm{sk}_{\mathrm{cyclic}}E$) that captures the reflected light from visual scene surface shapes. Every vortex cycle has a generator a (denoted by $\langle a \rangle$), where a is the vertex of an edge in the path between vertex a and any other vertex in the cycle. A simplifying assumption made here is that every sequence of edges is a multiple of the edge that begins with vertex a. For more about generators, see Section 2.2.

Example 3. Sample Barycentric Vortex Cycle on an Alexandroff Nerve.
Let $\mathrm{sk}_{\mathrm{cyclic}}\boldsymbol{E}$ be a vortex cycle drawn on the barycenters of a filled Delaunay triangle as shown in Fig. 4. Many other examples of barycentric vortex cycles are shown in Fig. 7. ■

H. Edelsbrunner and J.L Harer (Edelsbrunner & Harer, 2010, §III.2, p. 59) that, in general, an *Edelsbrunner-Harer nerve* complex is a collection of sets that have nonempty intersection.

Construction of a Barycentric Vortex Nerve:
For the triangles bordering an Alexandroff nerve Nrv$E$, construct a filled vortex cycle $\mathrm{sk}_{\mathrm{cyclic}}E'$ on the barycenters of the triangles. Each edge of $\mathrm{sk}_{\mathrm{cyclic}}E'$ is on a half plane that covers the common vertex of the Alexandroff nerve Nrv$E$.

Lemma 1. *A collection of nesting, overlapping filled vortexes is an Edelsbrunner-Harer nerve complex.*

Proof. Let $\mathrm{sk}_{\mathrm{cyclic}}E, \mathrm{sk}_{\mathrm{cyclic}}E'$ be filled vortex cycles on Alexandroff nerve Nrv$E$. $\mathrm{sk}_{\mathrm{cyclic}}E, \mathrm{sk}_{\mathrm{cyclic}}E'$ are nesting vortexes, since vortex $\mathrm{sk}_{\mathrm{cyclic}}E$ is in the interior of $\mathrm{sk}_{\mathrm{cyclic}}E'$. We have

$$\mathrm{sk}_{\mathrm{cyclic}}\mathrm{Nrv}E = \{\mathrm{sk}_{\mathrm{cyclic}}E, \mathrm{sk}_{\mathrm{cyclic}}E' : \mathrm{sk}_{\mathrm{cyclic}}E \cap \mathrm{sk}_{\mathrm{cyclic}}E' \neq \emptyset\},$$

since each vortex cycle is filled and the portion of the plane occupied by $\mathrm{sk}_{\mathrm{cyclic}}E'$ includes $\mathrm{sk}_{\mathrm{cyclic}}E$. Hence, $\mathrm{sk}_{\mathrm{cyclic}}\mathrm{Nrv}E$ is an Edelsbrunner-Harer nerve complex. □

For each video frame, it is possible to extend outward from a barycentric Alexandroff vortex cycle to form multiple nesting filled vortex cycles, one inside the other. In that case, the collection of vortex cycles form a large vortex nerve.

Theorem 1. *A collection of nesting, overlapping filled vortex cycles on a triangulated video frame is an Edelsbrunner-Harer nerve complex.*

Proof. Let $\mathrm{sk}_{\mathrm{cyclic}}\mathrm{Nrv}E$ be a collection of nesting, overlapping filled vortex cycles on a video frame. From Lemma 1, we have

$$\mathrm{sk}_{\mathrm{cyclic}}\mathrm{Nrv}E = \left\{\mathrm{sk}_{\mathrm{cyclic}}E \in \mathrm{sk}_{\mathrm{cyclic}}\mathrm{Nrv}E : \bigcap \mathrm{sk}_{\mathrm{cyclic}}E \neq \emptyset \neq \emptyset\right\}.$$

Hence, $\mathrm{sk}_{\mathrm{cyclic}}\mathrm{Nrv}E$ is a nerve complex. □

Example 4. Sample Video Fame Vortex Nerve Complexes.
A trio of video frame vortex nerve complexes are shown in Fig. 5. In Fig. 5.1, for example, a collection of 4 nesting, overlapping vortexes are shown with

vortex.1 *(innermost* **vortex** *) with blue edges with 12 vertices. There is a cusp filament attached between the 12 vertices on the blue vortex and*

vortex.2 *(* **vortex** *) with more than 20 vertices. Again, there is a cusp filament attached between more than 20 vertices on the blue vortex and*

vortex.3 *(* **vortex** *) with more than 30 vertices. Again, there is a cusp filament attached between more than 30 vertices on the blue vortex and*

vortex.4 *(* **vortex** *) with more than 30 vertices.*

The vortex nerve in Fig. 5.2 consists of a pair of overlapping vortexes with 12 cusp filments attached between the vortexes. A pair of vortex nerves on the same triangulated video frame are shown in Fig. 5.3. ■

2.2. Cyclic groups representing video frame vortex nerves.

Let sk$E$ be a filled vortex (*i.e.*, also called a skeleton) on a triangulated video frame. The vertices in vortex sk$E$ are path-connected. This means that there is path between every pair of vertices in sk$E$. In addition, each sk$E$ is bi-directional in a vortex nerve. So, for example, if vertices p, q are on sk$E$, a movement (traversal) from p to q is represented by $p + q$ and a reverse traversal is represented by $-q + p$.

The + between path edges reads **attach to**. No movement is represented by $p + (-p) = 0p$. In effect, every member p in sk$E$ has an inverse $-p$ and $0p$ represents an identity element in an algebraic group view of sk$E$. Notice that + operation is Abelian. To see this, do addition modulo 2 on the coefficients in a movement from p to q, *e.g.*,

$$p + q \longmapsto 1 + 1 \mathrm{mod} 2 = 0, \text{ and}$$
$$q + p \longmapsto 1 + 1 \mathrm{mod} 2 = 0.$$

For such a group, we write (sk$E$, +) (called a *cyclic Abelian group*). A *generator* of skeleton sk$E$ (denoted by $\langle a \rangle$) of such a group is a minimum length edge with a distinguished, starting vertex $a \in \mathrm{sk}E$. Let V be an ordered set of k path-connected vertices in vortex sk$E$, namely,

$$V = \overbrace{\{v_0, v_1, \ldots, v_i, \ldots, v_{k-1}\}}^{k \textbf{ ordered vertices}}.$$

$$\langle a \rangle = \overbrace{\qquad\qquad}^{\textbf{generator } \langle a \rangle \textbf{ = minimum edge-length}} \overbrace{\|v_1 - v_0\|}.$$

Example 5. Sample Generator of a Cyclic Group.
Let generator $\langle a \rangle$ represented by vertex 0b in vortex skB in Fig. 1, which is the starting vertex in a minimum

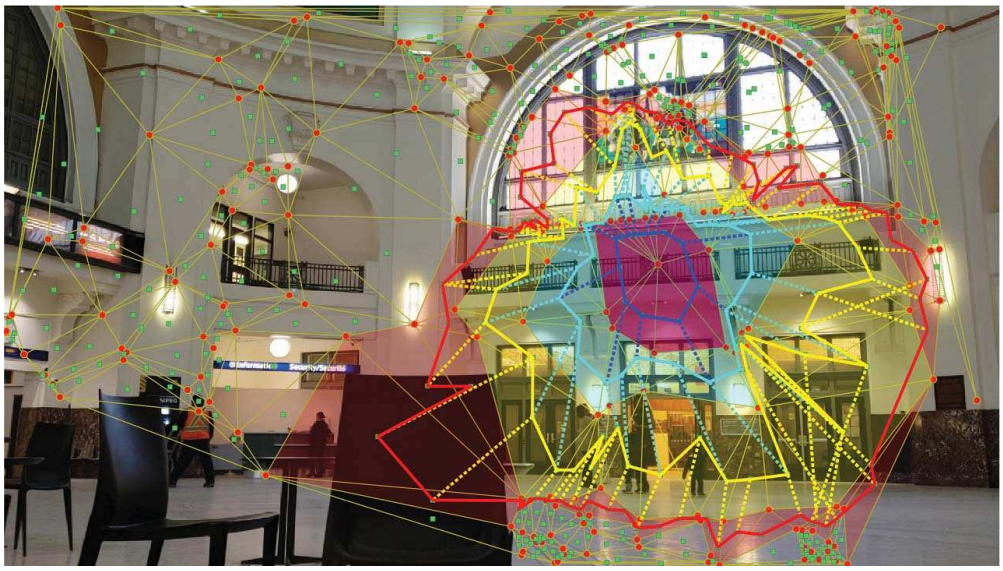

5.1: Frame 4-vortex nerve

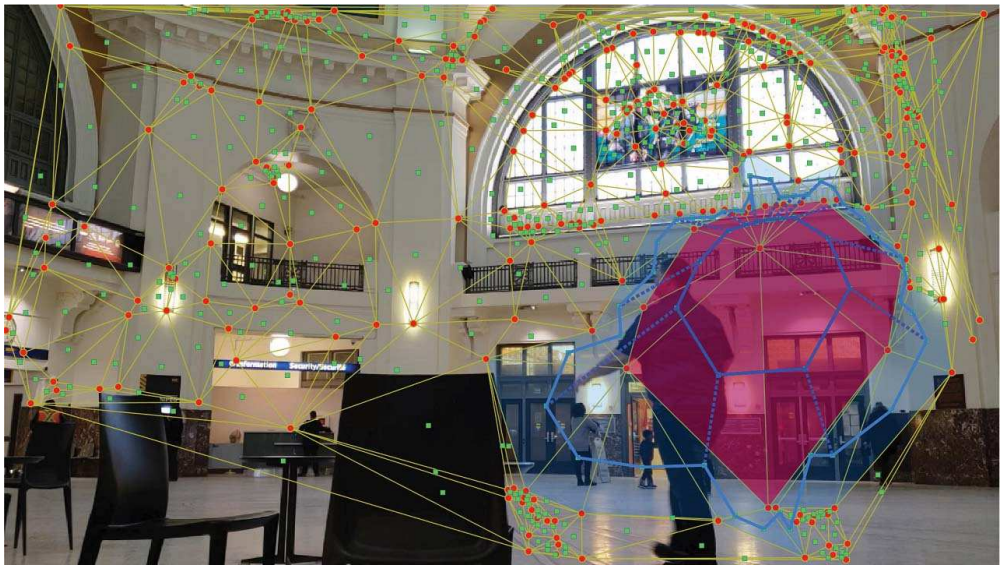

5.2: Frame 2-vortex nerve

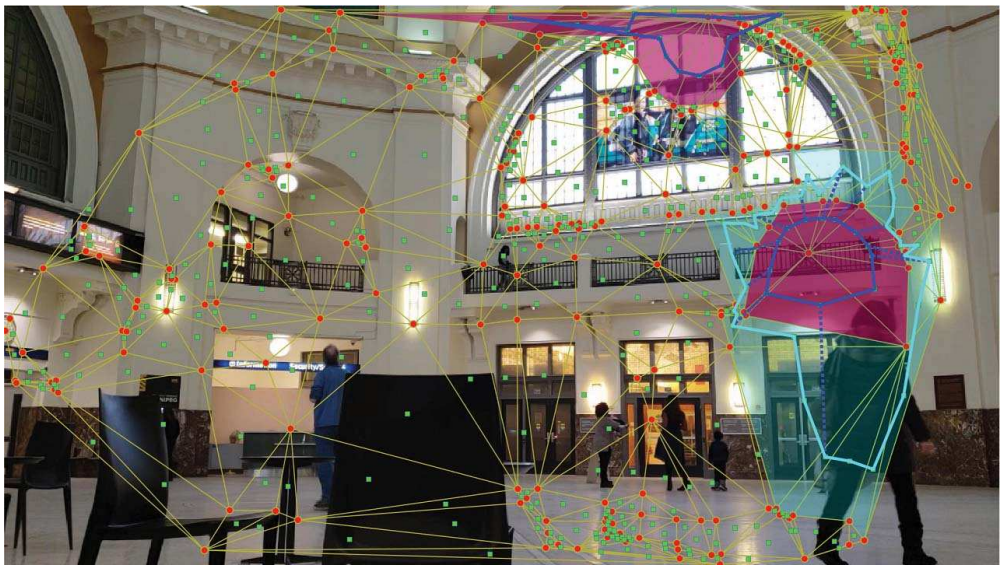

5.3: Frame dual vortex nerves

Figure 5. Sample triangulated frames for video 1.

length edge $\widehat{0b1b}$. *Then, for example, vertex* $p2 \in skB$ *can written as a multiple of edge* $\widehat{0b1b}$, i.e.,

$$p2 = \widehat{0b1b} + \widehat{1b2b} + \cdots + \widehat{8b9b}$$
$$\overbrace{\longmapsto 1b + 1b + \cdots + 1b}^{\textbf{maps to a multiple of generator } \langle b \rangle}$$
$$= 9b. \quad \blacksquare$$

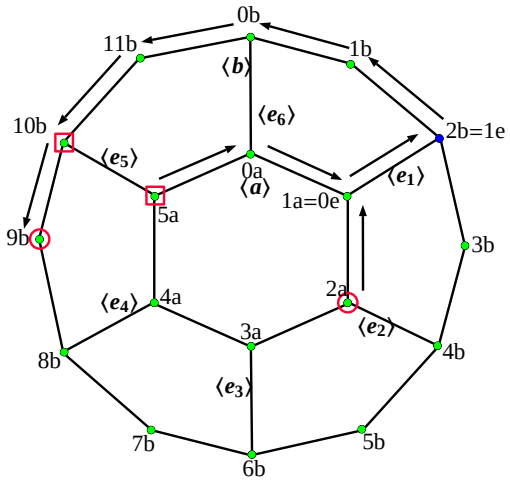

Figure 6. Sample Vortex Nerve with 6 filaments attached between vortexes

2.3. Cyclic groups for filament edges between vortexes.

An edge attached between the inner and outer vortexes in a vortex nerve is called a filament, which has a cyclic group representation. Let e be a filament (denoted by file) between a pair of vortexes. A filament is bi-directional, *i.e.*, a filament can be traversed in either the forward (+e) or reverse direction (-e) relative to a starting vertex on the filament. Hence, a filment is its own inverse and we write

$$\overbrace{e + (-e) = e - e = 0.}^{\textbf{no traversal of filament } e}$$

Notice that traversal of file k times is the same as traversing filament e one time. Hence,

$$\overbrace{e + \cdots + e = e + e = e.}^{\textbf{filament } e \textbf{ is an identity element}}$$

Obviously, the traversal operation + is Abelian, $e + e' = e' + e$. Consequently, a filament with the binary operation + is an Abelian group, represented by (filament $e, +$). Every filament is its own generator. A filament Abelian group is also written as $(\langle e \rangle, +)$.

Example 6. Multiple Filaments Attached Between Vortexes.
Let a vortex nerve NrvE contains 6 filaments attached between the vortexes $\langle a \rangle, \langle b \rangle$ *is shown in Fig. 6, each*

with its own generator, namely,

$$\overbrace{\langle e_1\rangle, \langle e_2\rangle, \ldots, \langle e_6\rangle}^{\textbf{Six Filament Groups}}.$$

Notice that each pair of vertices in NrvE is path-connected. This means that each member of the vortex nerve can be written as a linear combination of the generators. For example, consider the pair of vertexes $2a, 0b$*. Then we have*

$$0b = \overbrace{2a + 0e + 1e + 1b + 0b}^{\textbf{Traverse edges starting at } 2a \textbf{ and ending with } 0b}. \quad \blacksquare$$

From Example 6, we have a way of representing a vortex nerve in terms of its generators. That is, we can write

$$\overbrace{\text{Nrv}E = \{\langle a\rangle, \langle e_1\rangle, \langle e_2\rangle, \ldots, \langle e_6\rangle, \langle b\rangle\}}^{\textbf{Vortex nerve is a collection of generators}}.$$

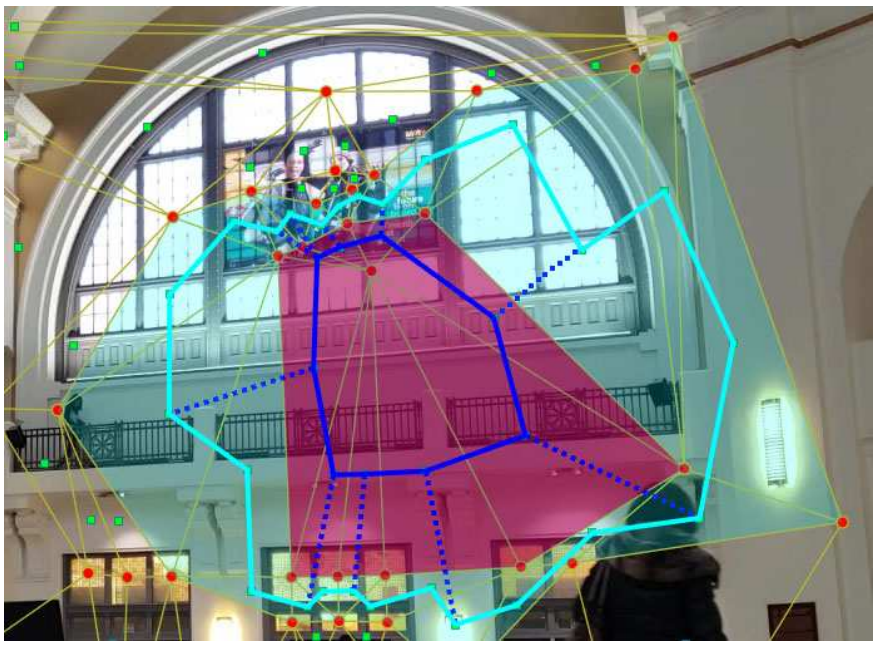

Figure 7. Barycentric vortex nerve on a triangulated video frame

2.4. Betti number for a vortex nerve on a triangulated video frame.

Notice that a vortex nerve is a collection vortexes that are attached to each other. This means that every pair of vertices in a vortex nerve is path-connected. Also notice that each skeletal vortex in a vortex nerve is represented by a cyclic Abelian group with its own generator. In effect, every vortex nerve has a free Abelian group representation. A **free abelian group** is an Abelian group with multiple generators, *i.e.*, every element of the group can be written as $\sum_i g_i a$ for generators $\langle g_i\rangle$ in G.

A Betti number is a count of the number of generators (rank) in a free Abelian group (Giblin, 2016, p. 151). This observation coupled with what we know about the cyclic Abelian group representation of

each skeletal vortex and of each bi-directional sequence of edges attached between the vortexes, leads to the following result.

Theorem 2. (Peters, 2020, §4.13, p. 263).
Let $\mathcal{B}(sk_{cyclic}NrvE)$ be the Betti number of $sk_{cyclic}NrvE$. A free Abelian group representation of $sk_{cyclic}NrvE$ includes k generators of cusp filament cyclic groups and two generators of the pair of the pair of cyclic groups representing the nesting, non-concentric nerve vortexes. Hence, $\mathcal{B}(sk_{cyclic}NrvE) = k + 2$.

Example 7. *A sample optical vortex nerve on the triangles of an Alexandroff nerve on a triangulated video frame, is shown in Fig. 7. Briefly, notice that there is a pair of nesting, non-concentric vortexes with 9 attached between inner and outer vortex vertexes, each with its own generator. Hence, from Theorem 2, the Betti number equals 2 + 10 = 12 for this sample nerve.* ■

2.5. Maximal Nerve Complexes (MNCs)

Of particular interest among all of the possible Alexandroff nerves on a triangulated video frame are those nerves that have a maximal number of triangles attached to a particular vertex. In a triangulation of frame centroids, a *maximal nerve complex* (MNC) has the highest number of centroids surrounding the common centroid at its center. Each of the MNC vertexes is a centroid of an image dark region (hole). For this reason, an MNC has the highest number of dark regions (holes) in the triangulation of video frame centroids. Also, the barycenters of the triangles on an MNC are between image holes, since each barycenter is in that part of a triangle between the centroids on frame dark regions. Hence, connected barycenters model paths for light from either reflected or refracted light from visual scene surface shapes recorded in a video frame. That is, the edge between a pair of barycenters stretches across a visual scene surface where there is reflected or refracted light. Consequently, with a vortex nerve on an MNC, we will find the highest concentration of contrasting light and dark regions in an image. It is well-known that a concentration of surface holes defines a surface shape. In other words, a surface shape represented by an MNC will have the highest definition, *i.e.*, highest concentration of holes pinpointed by their centroids.

Example 8. Sample Video Frame MNC.
A sample video frame MNC is shown the majenta-coloured region in Fig. 7. ■

3. Betti Number-Based Video Barcode

A Betti number-based video *barcode* is a pictograph that records one or more occurrences of Betti numbers derived from vortex nerves across sequences of triangulated frames. In our case, a frame Betti number tells us the number of generators in the frame vortex nerve. A repetition of the same Betti number across a sequence of consecutive frames tells us that there is a similar shape outlined by a vortex nerve that recurs on the frames.

In the video barcode introduced in the paper, there is a 1-to-1 correspondence between a frame number and a Betti number. There can be more than one vortex nerve on a frame. Hence, a frame with more than one Betti number will result in the more than one bar in the same column of the video barcode. The steps to construct a video barcode are given in Alg. 2.

Example 9. Sample Video Barcodes.
Sample video barcodes are given in Fig. 8.1 and Fig. 8.2. A persistent video frame Betti number is represented by a row of contiguous bars. ■

Algorithm 2: Video Barcode Construction Method

input : A video *Im* of size $w \times l$ and f frames
output: A triangulated video $w \times l$ and f frames

while *count* $< f$ **do**
  count ← count + *1*;
  Read the video and get frame(*count*).;
  matCentroids ← `skelSeedPoints(`frame(*count*)`)` ;
  triDelaunay ← *Perform Delaunay triangulation on* matCentroids.;
  `plot(`triDelaunay`);`
  mncNode ← *Calculate the most common node in* triDelaunay ;
  matBarycenters ← *Calculate barycenters of triangles in* triDelaunay ;
  mncBarycenters ← *Select barycenters surrounding* mncNode *from* matBarycenters ;
  `plot(`matBarycenters`);`
  bettyNo (count)(j) =1;
  while *i* < `length(`*mncNode*`)` **do**
    kvortex (i)(1) ← mncBarycenters;
    j ← *1*;
    while `polygon(`spkComplex *(i)(j)*`)` *encapsulate* spkComplex(*i*)(*j* − 1) **do**
      kvortex (i)(j) ← *Calculate immediate neighboring triangles*;
      spkComplex (i)(j) ← *Select barycenters of* kvortex *(i)(j) from* matBarycenters ;
      `plot(polygon(`spkComplex *(i)(j)*`))`;
      filaments ← *Connect each vertices of* spkComplex *(i)(j-1) to vertices in* spkComplex *(i)(j)* ;
      `plot(`filaments`);`
      bettyNo (count)(j) = bettyNo (count)(j) + `length(`spkComplex *(i)(j-1)*`)` +1;
  Write frame ;
`plot(`bettyNo`);`

The gaps between the sequences of contiguous bars are important. Since each column in a video barcode corresponds to a video frame, a barcode row containing a sequence of contiguous bars corresponds to sequence of video frames that we can identify. As a result, each row containing persistent Betti numbers leads to the production of a new video in which only frames containing vortex nerves with similar shapes appear in the video. Each row video containing a persistent surface shape give us a closer look at the minute changes in surfaces covered by a vortex nerve with the same Betti number. This leads to the following provable observations.

Observation 1. *A Betti number-based video barcode row with no gaps indicates the presence of a vortex nerve with approximately the same shape in each video frame.* ■

Observation 2. *A Betti number-based video barcode row with large gaps between occurrences of a Betti number indicates the presence of dissimilar vortex nerve with dissimilar shapes in large number of video frames.* ■

A pair of vortex nerves $\mathrm{sk}_{\mathrm{cyclic}}\mathrm{Nrv}E, \mathrm{sk}_{\mathrm{cyclic}}\mathrm{Nrv}E'$ are descriptively close, provided the vortex nerves have

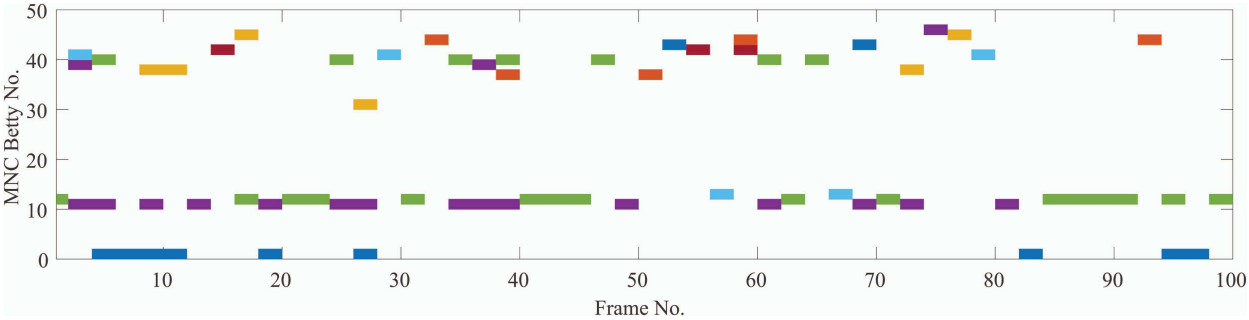

8.1: Barcode for a triangulated video

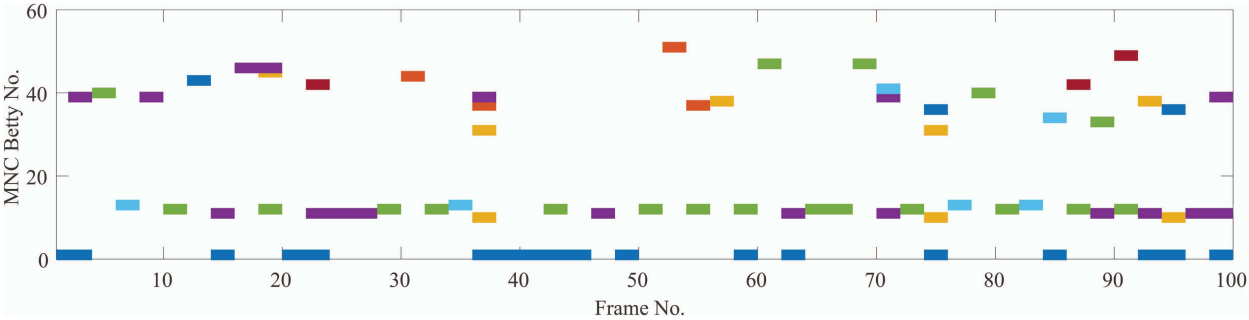

8.2: Barcode for a 2nd triangulated video

Figure 8. Sample Video Ghrist Barcodes for Two Videos

the same description, *i.e.*, a feature vector $\Phi(\mathrm{sk}_{\mathrm{cyclic}}\mathrm{Nrv}E)$ that describes $\mathrm{sk}_{\mathrm{cyclic}}\mathrm{Nrv}E$ will match the feature vector $\Phi(\mathrm{sk}_{\mathrm{cyclic}}\mathrm{Nrv}E')$. This is leads to the following observation.

Observation 3. *A Betti number-based video barcode row with a persistent Betti number across the video frames implies the presence of descriptively close vortex nerves on the frames.* ■

4. Time complexity Analysis

Fig.9 shows the results of the time complexity analysis for the algorithm. In order to calculate the theoretical time complexity several assumptions were made. The time taken for built-in functions were not considered; for example time taken to import the video frame, save the triangulated frames, initializing variables, inner working of loops etc. Addition, Subtraction, Multiplication, Division were taken as 4 different calculations.Furthermore, allocation of values and array search function were considered to be one calculation.

The theoretically obtained time complexity in terms of big O notation was mn^2 where m is the number of MNCs and n is the number of centroids.

In order to obtain the actual time complexity plot, randomly generated points were used. This ensures that the generated points are not based on a particular image and will give more generic results. To plot the two graphs in the same plot, a scaling factor k was calculated. So the final theoretical graph shown in Fig.9 is in the form of kmn^2. The value of k was experimentally found to be $1.0526e^{-4}s$.

The theoretical graph is shown in green dotted line. The actual time complexity is shown using the blue solid line. The number of MNCs that were generated are shown by the gray stem plot. The red dotted line shows the kn^2 graph where the MNC number was not considered. It is evident from the plots that both

number of centroids and the number of MNCs affects the time complexity of the algorithm. Furthermore, the kmn^2 graph follows the real time complexity graph very closely.

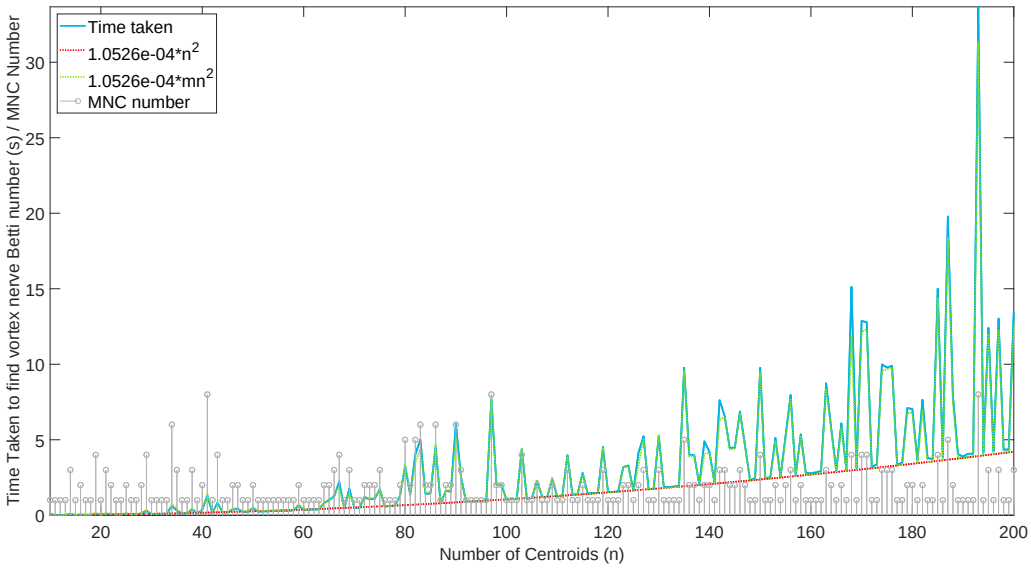

Figure 9. Time complexity.

5. Conclusion

A video, Betti nuumber-based form of Ghrist barcode has been introduced in this paper. This form of Ghrist barcode is useful in tracking the persistence of surface shapes recorded in sequences of video frames.

References

Ahmad, M.Z. and J.F. Peters (2018). Maximal centroidal vortices in triangulations. a descriptive proximity framework in analyzing object shapes. *Theory and Applications of Math. & Comp. Sci.* **8**(1), 38–59. ISSN 2067-6202.

Alexandroff, P. (1926). Simpliziale approximationen in der allgemeinen topologie. *Mathematische Annalen* **101**(1), 452–456. MR1512546.

Alexandroff, P. (1965). *Elementary concepts of topology*. Dover Publications, Inc.. New York. 63 pp., translation of Einfachste Grundbegriffe der Topologie [Springer, Berlin, 1932], translated by Alan E. Farley , Preface by D. Hilbert, MR0149463.

Alexandroff, P. and H. Hopf (1935). *Topologie. Band I*. Springer. Berlin. Zbl 13, 79; reprinted Chelsea Publishing Co., Bronx, N. Y., 1972. iii+637 pp., MR0345087.

Alexandrov, P.S. (1956). *Combinatorial Topology*. Graylock Press. Baltimore, Md, USA. xvi+ 244 pp. ISBN: 0-486-40179-0.

Apostol, T. and M.A. Mnatsakanian (2000). Finding centroids the easy way. *Math Horizons* **8**(1), 7–12.

Berger, M. (1994). *Geometry. I.*. Universitext, Springer-Verlag. Berlin. Translated from the 1977 French original by M. Cole and S. Levy, xiv + 427 pp., ISBN: 3-540-11658-3,.

Edelsbrunner, H. and J.L. Harer (2010). *Computational Topology. An Introduction*. Amer. Math. Soc.. Providence, RI. xii+241 pp. ISBN: 978-0-8218-4925-5, MR2572029.

Edelsbrunner, H., D. Letscher and A. Zomorodian (2000). Topological persistence and simplification. In: *41st Annual Symposium on Foundations of Computer Science*. pp. 454–463. IEEE Comput. Soc. Press. Los Alamitos, California. MR1931842.

Edelsbrunner, H., D. Letscher and A. Zomorodian (2001). Topological persistence and simplification. *Discrete Comput. Geom.* **28**(4), 511–533. MR1949898.

Ghrist, R. (2008). Barcodes: the persistent topology of data. *Bull. Amer. Math. Soc. (N.S.)* **45**(1), 61–75. MR2358377.

Ghrist, R.W. (2014). *Elementary Applied Topology*. University of Pennsylvania. vi+269 pp. ISBN: 978-1-5028-8085-7.

Giblin, P. (2016). *Graphs, surfaces and homology, 3rd Ed.*. Cambridge University Press. Cambridge, GB. xx+251 pp. ISBN: 978-0-521-15405-5, MR2722281, first edition in 1981, MR0643363.

Le, B., H. Nguyen and D. Tran (2014). A robust fingerprint watermark-based authentication scheme in h.264/avc video. *Vietnam J Comput Sci* **1**, 193–206. DOI: 10.1007/s40595-014-0021-x.

Perea, J.A. (2018). A brief history of persistence. *arXiv* **1809**(036249), 1–11.

Peters, J.F. (2017). Proximal planar shape signatures. Homology nerves and descriptive proximity. *Advan. in Math: Sci. J* **6**(2), 71–85. Zbl 06855051.

Peters, J.F. (2018*a*). Proximal planar shapes. correspondence between triangulated shapes and nerve complexes. *Bulletin of the Allahabad Mathematical Society* **33**, 113–137. MR3793556, Zbl 06937935, Review by D. Leseberg (Berlin).

Peters, J.F. (2018*b*). Proximal vortex cycles and vortex nerve structures. non-concentric, nesting, possibly overlapping homology cell complexes. *Journal of Mathematical Sciences and Modelling* **1**(2), 56–72. ISSN 2636-8692, www.dergipark.gov.tr/jmsm, See, also, https://arxiv.org/abs/1805.03998.

Peters, J.F. (2020). *Computational Geometry, Topology and Physics of Digital Images with Applications. Shape Complexes, Optical Vortex Nerves and Proximities*. Springer Int. Pub. AG. Cham, Switzerland. vii+563, *in press*.

Peters, J.F. and S. Ramanna (2018). Shape descriptions and classes of shapes. A proximal physical geometry approach. In: *Advances in feature selection for data and pattern recognition* (B. Zielosko U. Stańczyk and L.C. Jain, Eds.). pp. 203–225. Springer. MR3895981.